Recurrent droughts increase risk of cascading tipping events by outpacing adaptive capacities in the Amazon rainforest

Nico Wunderling[a,b,c,1] , Arie Staal[d,e] , Boris Sakschewski[a], Marina Hirota[f,g] , Obbe A. Tuinenburg[d,e], Jonathan F. Donges[a,e] , Henrique M. J. Barbosa[h,i,1] , and Ricarda Winkelmann[a,b,1]

Tipping elements are nonlinear subsystems of the Earth system that have the potential to abruptly shift to another state if environmental change occurs close to a critical threshold with large consequences for human societies and ecosystems. Among these tipping elements may be the Amazon rainforest, which has been undergoing intensive anthropogenic activities and increasingly frequent droughts. Here, we assess how extreme deviations from climatological rainfall regimes may cause local forest collapse that cascades through the coupled forest–climate system. We develop a conceptual dynamic network model to isolate and uncover the role of atmospheric moisture recycling in such tipping cascades. We account for heterogeneity in critical thresholds of the forest caused by adaptation to local climatic conditions. Our results reveal that, despite this adaptation, a future climate characterized by permanent drought conditions could trigger a transition to an open canopy state particularly in the southern Amazon. The loss of atmospheric moisture recycling contributes to one-third of the tipping events. Thus, by exceeding local thresholds in forest adaptive capacity, local climate change impacts may propagate to other regions of the Amazon basin, causing a risk of forest shifts even in regions where critical thresholds have not been crossed locally.

climate tipping elements | Amazon rainforest | tipping cascades | network dynamics | droughts

The Amazon rainforest is the most biodiverse terrestrial ecosystem and plays a fundamental role in regulating the global climate (1, 2). However, human-induced impacts and climatic extremes are increasingly threatening the forest's integrity and the services it provides (3, 4). Furthermore, forest changes might not be gradual, but could be rather abrupt due to nonlinear interactions, as suggested by simulation studies (5, 6), data-based approaches (7, 8), conceptual models (9–11), and long-term experiments (12, 13). Therefore, parts of the Amazon rainforest may be bistable, meaning that they could tip to an alternative state of low tree cover. The Amazon has been identified as a climate tipping element (14) and may be in danger of approaching or exceeding its tipping point (3, 15, 16). While a system-wide tipping point remains debated, local feedbacks can lead to alternative stable states (local-scale tipping elements) (7, 8).

The transgression of such a local-scale tipping point could, for instance, be caused by declining average precipitation levels or with increasing dry spells and severity of extreme droughts (17–19). Changes in precipitation regimes are already occurring over southern Amazon regions where the length of the dry season has been increasing by 1 mo since the mid-1970s (19, 20). This finding is largely consistent with several further data-based, artificial-intelligence–based, and observation-based studies from regional to Amazon basin-wide investigations, suggesting a later onset and earlier demise of the wet season due to changes in the South American Monsoon System (21–25). At the same time a bipolar trend has been found: While many regions in the Amazon basin have become drier overall, regions in the western part of the Amazon basin have received more rainfall during the last decades (26–28).

A lengthening and strengthening of the dry season in the southern Amazon basin have also been confirmed by modeling studies from CMIP5 (Coupled Model Intercomparison Project Phase 5) simulations as well as empirical precipitation models (19, 29, 30). In regions where dry periods last longer than 4 mo, it is likely that vital functions of the Amazon rainforest are impacted (3, 29). Those are also the parts of the rainforest that are losing resilience fastest since the beginning of this century, as a recent study suggests (16).

The Amazon is not a uniform forest as trees can adapt to local long-term water stress conditions (17). Ecologically speaking, such adaptations may be translated as different drought tolerance strategies (31), such as variable rooting depth systems (32–34) and embolism resistance (35), which are likely to define more dry-affiliated plant community assemblages (36). Indeed, plant recruitment has been shifting toward more dry-affiliated community assemblages in response to dry season intensification (37). Such local-scale

Significance

The Amazon rainforest is among the Earth's climate tipping elements. Under ongoing global warming, the frequency of severe droughts such as in 2005 and 2010 is projected to increase strongly, up to the point where these droughts may become the new climate normal in the second half of this century. Taking into account the adaptation of the forest to past environmental conditions, we find that nonlinear thresholds in the hydrological balance of the rainforest might be exceeded under drier future conditions, leading to self-amplified forest transitions. Thereby, we reveal that the lack of moisture recycling in some parts of the forest can be propagated downwind by the reduction of atmospheric moisture transport, resulting in approximately one-third of all tipping events.

heterogeneity can determine a variety of thresholds in plant mortality in response to current and future changes in rainfall regimes. Furthermore, a higher diversity in hydraulic traits among plants and trees has been shown to lead to larger resilience against droughts, and hydraulic adaptation is key to tropical forest resilience (31, 38, 39). Forest adaptation can therefore ensure that plants will operate close to their physiological maximum, but this creates vulnerabilities when the climate changes faster than the ecosystem can respond (40). In the case that trees die back locally, these climatic changes can be propagated by the forest itself, because trees contribute to precipitation regionally through the atmospheric moisture recycling feedback (41).

Trees recycle part of the precipitated water through atmospheric moisture recycling (41). They do so by extracting water from deeper soil levels and releasing it through their leaves (transpiration) and by intercepting precipitation that can evaporate before infiltrating the soil (interception evaporation). The total amount of atmospheric moisture recycling accounts for up to half of the precipitation over the Amazon basin and moisture is recycled up to six times (42, 43). Thus, the rainforest depends on itself, because precipitation and evapotranspiration recycling cycles propagate spatially through the basin and promote cascading forest development (42). The positive interplay between the forest and regional precipitation also implies that local perturbations can propagate in space via atmospheric moisture recycling (44, 45). Under deforestation, a strong reduction in this atmospheric recycling potential has been projected for the Amazon basin (46) and observed for the southern Amazon basin (45). The latter is a region that strongly depends on the additional water supply from recycling, illustrating the potential for cascading moisture effects throughout the Amazon rainforest. In other words, the Amazon rainforest can be considered as a network of local-scale tipping elements that are connected via atmospheric moisture recycling (9, 47).

As a result of state transitions, there would be a reduction of the atmospheric moisture transport between different parts of the Amazon. These, in turn, would decrease precipitation and increase water deficit downstream, exacerbating the tipping likelihood since the forest would then be closer to, or have crossed, its boundaries of physiological operation (9). Recent severe droughts such as in 2005 and 2010 already impacted the rainforest as revealed and analyzed by many different modeling (48, 49), comparative-historical (50–52), and empirical studies (53, 54). During these droughts, the trees decreased their investment in defense and maintenance, followed by a decrease in photosynthesis activity (55, 56).

Even though occasional strong droughts have long-lasting impacts on drought-induced tree mortality as well as further adverse drought legacies (57, 58), the rainforest might be able to withstand those incidental droughts. However, the adaptations of the forest may become insufficient to withstand permanent or prolonged increases in drier conditions (59). Indeed, observations from rainfall exclusion experiments in the Amazon rainforest (e.g., in the Tapajos or Caxiuaná National forest in Brazil) have reinforced this perspective (4, 60–62). The moisture profile in these rainfall exclusion experiments has been shifted from evergreen forest close to or beyond the transition edge to the savanna rainfall regime (4). While there has not been an instantaneous response of the forest to rainfall exclusion, it required only around 3 y before an increased tree mortality was observed (4, 12, 13). The reason has been argued to lie in the deep rooting systems of the trees, exploiting remaining soil moisture reserves (4). However, as soon as the long-term soil moisture has fallen below half of the potential water uptake ability of the trees, the tree mortality increases nonlinearly, especially among larger trees (12, 13). Overall, transitions from a rainforest to an alternative state were rare in the past, even though the Amazon has been significantly drier during the last glacial period (63). Although recent environmental changes have not been large enough to cause system-wide changes (64), some lines of evidence for potential state shifts (also outside of hydrology-induced transitions) are accumulating: 1) Parts of the Amazon rainforest in the south or closer to human settlements are found to lose resilience quicker than other parts (16). 2) Fire-induced transitions from forest to white-sand savanna states during the last 40 y have been found in several floodplains of the Amazon rainforest (65). 3) On top of that, vegetation conversions, i.e., community composition changes, from mesic to xeric species, have also been observed in multiple biomes globally, including in the Amazon (59, 66).

At the same time, models have projected that the major drought event of 2005 in the Amazon might occur more frequently under unmitigated global warming, up to 9 out of 10 y by 2060 (67, 68). This trend has been confirmed in the latest generation of CMIP6 models, which is largely consistent with the CMIP5 model generation (69, 70). High-emission scenarios ([Shared Socioeconomic Pathway] SSP3-7.0 and SSP5-8.5) project that precipitation may strongly decrease over the Amazon basin (69). Therefore, it seems indeed plausible that the future climate will resemble extreme drought events that occurred in the past 20 y with a strong epicenter in the southern and eastern Amazon rainforest basin (70).

By reconstructing dynamic atmospheric moisture recycling networks from the recent past, we can study how climate change may exceed the adaptation capacity of the forest and subsequently trigger local tipping points that cascade through the Amazon rainforest system. We integrate the following in a dynamic network model: 1) the local-scale tipping behavior of the Amazon forest, 2) the long-range coupling by atmospheric moisture flows, and 3) the adaptation of the forest to annual precipitation and droughts (Fig. 1). Specifically, we use a conceptual dynamical system to model local tipping points based on a local empirical relation between tree cover, mean annual precipitation (MAP), and dry season intensity (maximum cumulative water deficit [MCWD]).

We assume that the Amazon rainforest, on a level of $1° \times 1°$ grid cells, is adapted to its local values of MAP and MCWD over 20 y (1984 to 2003). This implies that parts of the forest that have experienced drier conditions in the past are also more tolerant to droughts in the future in our model, which is in line with earlier research (17, 37). The reason is that forest ecosystems have adapted to local environmental conditions by selecting functional traits that increase their overall ability to persist under natural climate variability and other stressors at play (31, 35, 71). We integrate the nonlinear forest ecosystems into our dynamical systems approach (*Materials and Methods*, Network of *Coupled Nonlinear Differential Equations*). To account for possible spatial variability and uncertainties (for instance, due to different soil properties), we create an ensemble of 100 members to investigate future drought conditions. This allows us to propagate the associated uncertainties thoroughly (*Materials and Methods*, Adaptation and Computation of Critical Thresholds and Ensemble Construction). Further, we construct the atmospheric moisture recycling network, which connects the different parts of the forest, using output from atmospheric moisture-tracking simulations and a global hydrological model (*Materials and methods*, Data) (42, 43).

It is possible that the future climatological rainfall regime would incorporate more extreme droughts and could resemble a permanent drought (68–70). Here, we focus on the effects of these future scenarios of droughts on the stability of parts of the Amazon rainforest. Hence, we do not look into other adverse influences
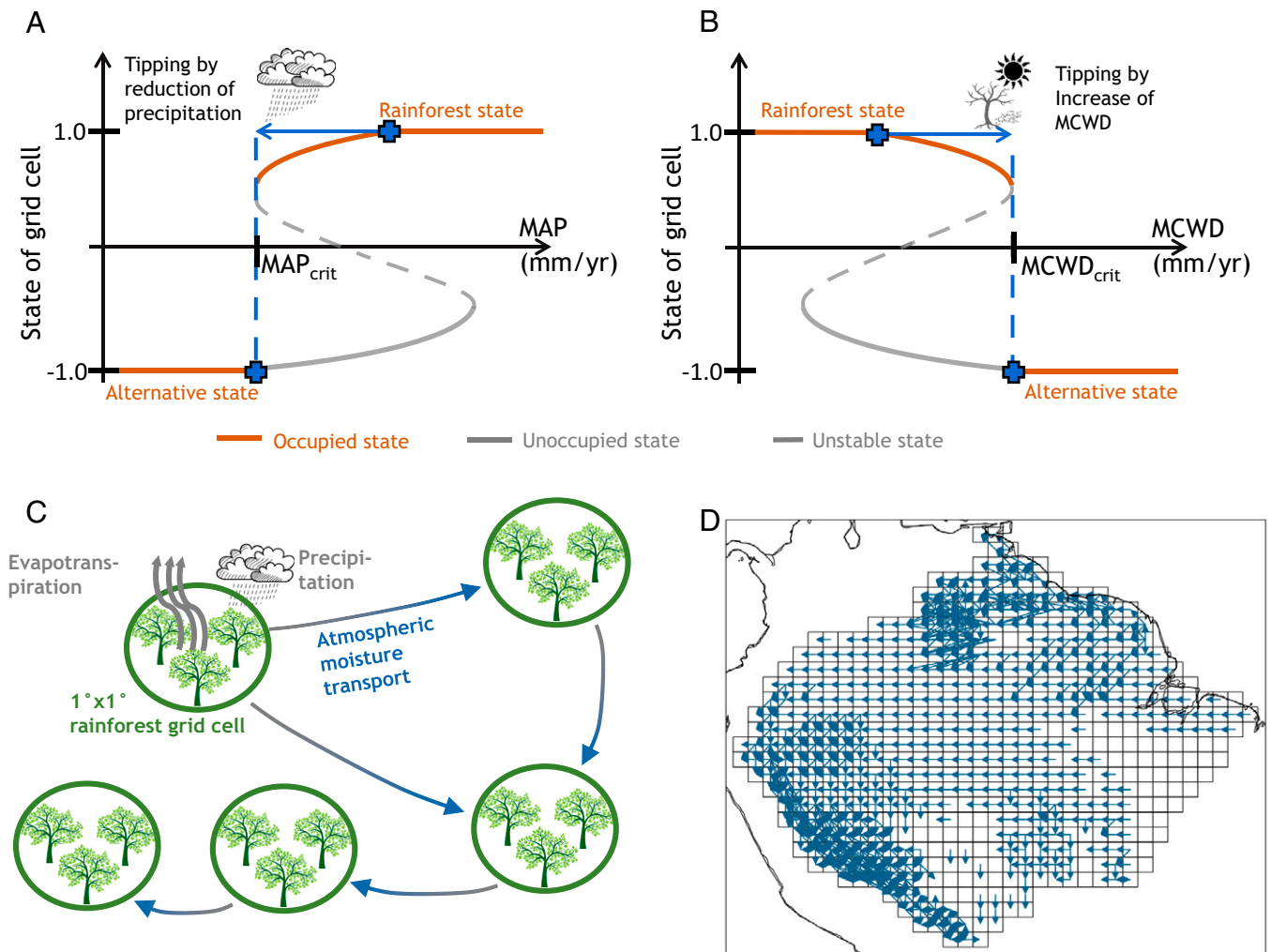
Fig. 1. Nonlinear effects and atmospheric moisture recycling network in the Amazon rainforest. (*A*) Dynamical property of each $1° \times 1°$ grid cell of the rainforest depicted as state of the grid cell versus MAP value. The state of the grid cell is limited by full forest cover (state value: 1.0) and an alternative state (open canopy, dry forest, savanna, treeless state value: -1.0). Between these two stable states, tipping occurs when the MAP value has fallen below its adaptation-specific MAP$_{crit}$ value. Since we are focusing on drought-induced tipping events from forest to nonforest states in this study, each cell is stable only on the brown states, but not on gray states (since we are not simulating a recovery of the forest). The gray dashed line represents the border separating the upper from the lower stable state (unstable manifold). The blue arrow depicts a potential reduction in precipitation that is sufficient to trigger a tipping event in this specific cell. (*B*) Same as in *A* for MCWD. (*C*) Exemplary atmospheric moisture recycling network, where each forest circle represents a $1° \times 1°$ grid cell, whose dynamics are shown in *A* and *B*. The different grid cells receive precipitation and experience evapotranspiration. The interaction between the different cells arises from the atmospheric moisture transport from evapotranspiration to precipitation. Through this mechanism, effects of reduced tree cover would be enhanced and tipping cascades are possible. (*D*) Atmospheric moisture recycling network for the hydrological year 2014 thresholded for links above 15 mm/y to maintain visibility. In the simulation results, links above 1 mm/y are used. The dominant flow direction comes from the Atlantic Ocean through easterly winds, reaches the Andes, and then bends southward along the Andes. Atmospheric moisture recycling links based on separate months and the dry/wet season can be found in *SI Appendix*, Figs. S1–S3 comparing the year 2014 with the extreme drought year 2010.

such as fire or deforestation. We explore a large range of different possible future climate states in the Amazon basin, building on realistic precipitation and evapotranspiration patterns from the recent past. Scenarios (i.e., future potential climate normals) are built by perpetuating the observed climatic anomalies from 2004 to 2014 in an equilibrium experiment. This also means that we do not look into the effects of single years. Compared to average conditions, the investigated future scenarios range from wet (e.g., 2009) to extremely dry conditions (two "droughts of a century": 2005 and 2010) (51, 72). Overall, this allows us to draw on realistic rainfall and evapotranspiration patterns based on earlier drought and nondrought years, instead of artificially and more arbitrarily making use of rainfall reduction experiments or climate model forecasts.

With our model experiments, we analyze the Amazon rainforest cells as local-scale tipping elements of the atmospheric moisture recycling network on a resolution of $1° \times 1°$ to assess their

impact on the Amazon-wide system stability (Fig. 1). Using this approach, we provide a bottom–up quantification of Amazon system stability to reveal where cascading effects of atmospheric moisture recycling have the potential to induce domino effects in forest cover loss.

Results

Tipping Due to Drier Conditions. To investigate a range of possible future water deficits and precipitation anomalies, we study the extent of the tipped area with respect to a range of future possible scenarios (climate normals), in which precipitation, evapotranspiration, and moisture transport patterns would consistently look like the year 2004, 2005, ..., 2013, or 2014. For that purpose, we use the so-called $\mathcal{Z}$-score measure (Eqs. **2** and **3**), which represents how many SDs the conditions are away from the mean of the control period (1984 to 2003). We find a correlation
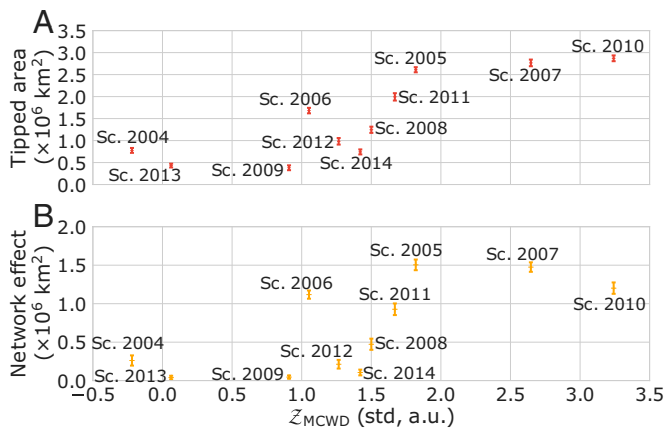
Fig. 2. Vulnerability of the rainforest against MCWD-based drought intensity. (*A*) The total tipped area is shown over the course of the normalized drought index based on the MCWD $\mathcal{Z}$ score. The tipped area represents the number of tipped cells in the model where each $1° \times 1°$ cell has an area of approximately 111×111 km^2. (*B*) Ratio of the tipped area due to network effects for each simulated scenario (new climate normal). This shows the effects of cascading transitions, which can reach orders of $1.5 \cdot 10^6$ km^2 depending on the evaluated scenario representing the hydrological years 2004 to 2014. The same analysis was performed for a MAP-based index (*SI Appendix*, Fig. S4). A sensitivity analysis for a stronger and a weaker moisture recycling network reveals the robustness of the obtained results (*SI Appendix*, Fig. S5). Sc., scenario.

between $\mathcal{Z}_{MCWD}$ and the tipped area, where a higher index reflects a larger tipped area (Fig. 2*A*). The future scenarios resembling the environmental constraints of the drought years 2005, 2007, and 2010 (i.e., if those years become the new climate normal) show the largest tipped area. The 2005 and 2010 droughts have been termed "once-in-a-century droughts" (72) and are together with 2007 the years with the highest drought conditions in our study period (2004 to 2014) (53). The scenario for the year 2010 shows the highest tipped area, closely followed by the 2005 and 2007 scenarios. The reason for this small difference between 2005 and 2010 might be that, while 2010 had the most extreme $\mathcal{Z}_{MCWD}$ index, 2005 shows the most extreme rainfall anomalies as measured by $\mathcal{Z}_{MAP}$ (*SI Appendix*, Fig. S4). Indeed 2005 had the highest rainfall anomalies within the 2004 to 2014 period when accounting only for rainfall that originated from oceanic moisture (i.e., neglecting recycled moisture) (42). Therefore, the increase of the tipped area with increasing $\mathcal{Z}_{MCWD}$ can be expected from our approach, suggesting that the investigation of tipping reasons and regional distributions of the drought patterns affecting local rainforest stability are the most important properties to investigate.

We separate local-scale tipping events into primarily induced tipping events from MAP or MCWD and secondary tipping induced by network effects (tipping cascades). Our model shows that up to $1.5 \cdot 10^6$ km^2 of the local tipping events are due to cascading effects from the atmospheric moisture recycling network depending on the scenarios' drought strength in terms of its Z_{MCWD} score (see network effects in Fig. 2*B*). The cascading effects are heterogeneously distributed among the investigated years, but are especially strong for the years that show the strongest drought signatures (i.e., future climate normals resembling 2005, 2007, and 2010). This is probably due to the fact that many cells are shifted toward their local tipping point and some of them across it. Consequently, with further reduction of atmospheric moisture transport, more cells in these scenarios transgress their calculated threshold. Therefore, if drought conditions intensify in the future, cascading tipping may increase disproportionally.

We also compared these results with the results of an only MAP-based normalized drought index $\mathcal{Z}_{MAP}$ (Eq. **3**) and find that

the future scenarios are considerably more adverse with respect to $\mathcal{Z}_{MCWD}$ than to $\mathcal{Z}_{MAP}$ (larger $\mathcal{Z}_{MCWD}$ values are reached compared to $\mathcal{Z}_{MAP}$; Fig. 2 and *SI Appendix*, Fig. S4). As a sensitivity experiment, we further assessed whether the extent of the tipped area will increase under different levels of the empirically obtained moisture transport strength and hence of the regional precipitation recycling ratio. We find robust results for both a 25% increase and a 25% decrease in the amount of water transported between pairs of forest cells (*SI Appendix*, Fig. S5), indicating that the results are not sensitive to uncertainties in the moisture flows.

Vulnerability Maps. Over the range of simulated scenarios, one region shows very high vulnerability and a second region moderate to high vulnerability (see vulnerability in Fig. 3*A*). These regions, located in the southeastern and southern to southwestern Amazon, are affected by a combination of MCWD anomalies and network effects. As expected from Fig. 2, the vulnerability patterns vary strongly from scenario year to scenario year (*SI Appendix*, Fig. S6), but the vulnerable regions in the southeast and southwest recur across many simulated scenario years.

We investigate the vulnerable regions in detail since, in our model, small changes in the state already have an impact on the atmospheric moisture recycling network, even though the respective cell does not qualitatively change state. This can be realized if the environmental conditions shift a rainforest cell close to, but not across, its local tipping point. We define a shift toward the local tipping point without an actual local tipping event as the closeness to tipping. We find that this closeness to local tipping is highest in the southeast of the Amazon basin and in the subsequent dominant downwind direction toward the Andes. The largest average shifts toward the local tipping point are located around and close to, but not directly at, the most endangered region in the southeast. The reason is that these cells are already tipped in most cases and do not contribute to the average closeness to tipping (Fig. 4*A*). However, this is expressed by the high variability among the ensemble members (see southeastern region and downwind in Fig. 4*B*).

Although local tipping points are thresholds by definition, our model indicates that effects on the Amazon forest–rainfall system already occur before MCWD or MAP reaches that point. This agrees with observations that droughts can have significant impacts on photosynthesis and evapotranspiration that may last for years (73, 74), which might in the end also affect the composition of the trees together with long-term effects on light availability. A threshold-only model cannot account for these effects on evapotranspiration. In our model, however, also partial state changes are accounted for; i.e., evapotranspiration scales with distance to the threshold of state change (tipping point). In other words, when a forest becomes drier, it generates less evapotranspiration, an effect that may cascade through the atmospheric moisture network and the entire forest system. Thus, even though our approach is conceptual, it allows us to identify which areas are most vulnerable to the invisible effect of the atmospheric moisture recycling network. The magnitude of this effect is on the order of 20 to 40% for many regions over the entire southern Amazon with a small region in the very southeast of the Amazon reaching 40 to 60%. This represents an average evapotranspiration decrease of ∼10 to 25% due to a shift toward the tipping point in these Amazon regions (Fig. 4*A*).

The Tipping Reason and Cascading Effects. We reveal that, over the whole set of simulated scenarios (2004 to 2014), the direct effect of MCWD-induced tipping is prevalent ($64.0 \pm 5.0\%$) over the $35.9 \pm 4.9\%$ that are due to cascading failure (Fig. 3*B*).
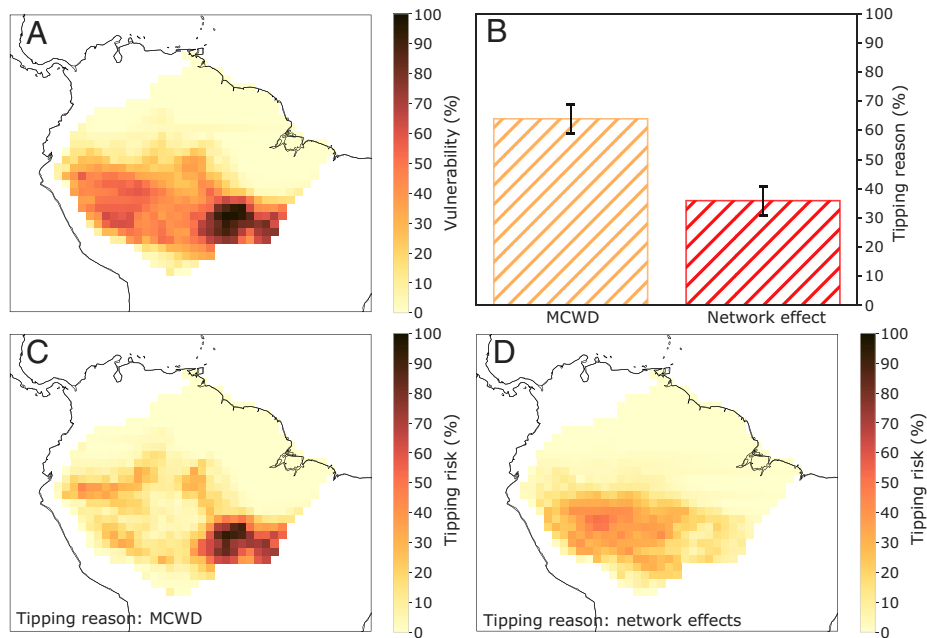
Fig. 3. Vulnerable regions and tipping reason. (*A*) The likelihood of tipping (vulnerability) as an average over all ensemble members and all evaluated scenarios resembling the hydrological years 2004 to 2014. The southeastern region is more vulnerable than other regions, but also the southern and southwestern regions are affected. In *SI Appendix*, Fig. S6, the yearly results can be found. (*B*) Overall tipping reason averaged over the entire Amazon basin with error bars as the SD over all years and all 100 ensemble members. A version separated into the future drought scenarios 2004, 2005, . . ., 2014 can be found in *SI Appendix*, Fig. S7 for all these potential future drought scenarios. MAP does not contribute to tipping events (probability is less than 0.1%) and is thus omitted here. (*C*) Regionally resolved tipping reason in the case that MCWD is the reason for a tipping event. (*D*) Same as for *C*, but showing network effects (cascading effects of the atmospheric moisture recycling network) are the tipping reason. Note that *A* is the sum of *C* and *D*.

Moreover, transitions of the forest due to MAP as a primary reason are nearly completely negligible since they are responsible for less than 0.1% of all local tipping events. The reason that MAP does not appear as an important cause for the emergence of tipping events may lie in the fact that cumulative water deficit is more sensitive to changes in the dry season conditions than annual precipitation. Therefore, the recent intensification of the dry season in parts of the Amazon (3) results in a larger $\mathcal{Z}$ score for MCWD than for MAP.

The cascading network effects are especially strong close to the region of direct MCWD-induced tipping and downwind from

that. MCWD is the most important reason for local tipping events in the southeast, whereas network effects are more important west of this region (Fig. 3 *C* and *D*). Overall, the region in the southeast is vulnerable with respect to MCWD since it has a moderate interannual variability (SD) of MCWD, while the intra-annual precipitation variability (mean) MCWD value is high (*SI Appendix*, Fig. S9 *C* and *D*). Together with increasing MCWD values in this region in the scenario period (2004 to 2014) compared to the calibration period (1984 to 2003), this leads to relatively many MCWD-induced tipping events, which can then spread out farther via network effects (tipping cascades).
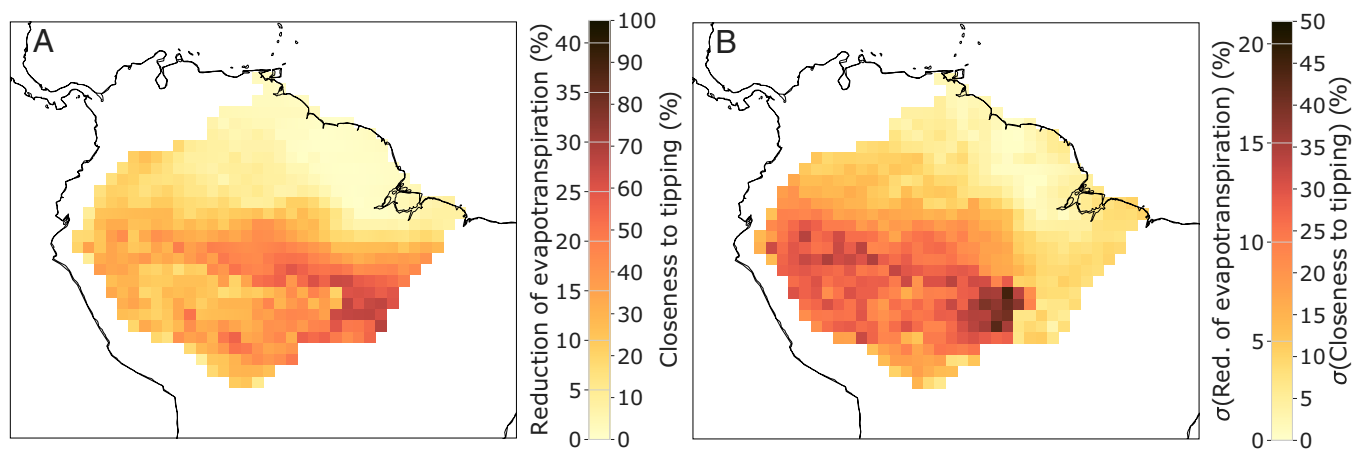
Fig. 4. Mean shift toward the tipping point (closeness to tipping). (*A*) Mean shift to the tipping point as an average over all ensemble members. It can be seen that the shift is larger in the southern part of the Amazon rainforest, meaning that this region is more vulnerable than the northern part. (*B*) SD of *A* over all ensemble members. Note that cells are accounted for only if the cell is not in the tipped regime in the respective simulation run. Since the closeness to tipping is translated linearly into a reduction of evapotranspiration, a second color bar indicates this change (*A*) together with its SD (*B*). A version separated into the future scenarios resembling the conditions from 2004 to 2014 can be found in *SI Appendix*, Fig. S8.

Discussion

Based on the assumption that tipping processes in the Amazon rainforest are conditioned by local to regional-scale adaptation, we estimate that tipping cascades can become responsible for around one-third ($35.9 \pm 4.9\%$) of the local tipping events in the Amazon rainforest. These cascades occur even when considering that the forest is adapted to local climatic conditions, which has not been considered by earlier studies (9). The reason is that drying is amplified by the atmospheric moisture losses that result from reduced evapotranspiration and, hence, moisture recycling, which in turn affects precipitation levels regionally. By constructing a dynamic network of forest cells connected by forest-induced atmospheric moisture flows, we reveal how and where the Amazon is vulnerable to tipping cascades. Local tipping due to fluctuating dry-season intensity (as measured by MCWD) is the dominant driver ($64.0 \pm 5.0\%$) compared to fluctuations in annual rainfall. With a potential increase of future extreme drought events (67–70), the average regional climate will be drier and some parts of the rainforest might thus be set under imminent risk of instability and could transition into a less-covered or non–forest-covered state. We uncover that local tipping events occur most frequently in the southeastern Amazon (Fig. 3).

A reduction in evapotranspiration has been found in earlier research and, in conjunction with a longer dry season and deforestation (44, 45), has been suggested to play out strongly in the southern Amazon, the same region where we find the largest fraction of local tipping events. Also, state-of-the-art CMIP6 models provide additional evidence that the Amazon rainforest is among the regions worldwide that would be hit hardest by climate-change–induced precipitation decreases and extreme drought increases (+200 to 300% until 2071 to 2100 in SSP3/SSP5 scenarios compared to 1851 to 1880) (69, 70). Particularly, the southern and eastern regions in the Amazon basin are projected to suffer from these intensified droughts (70). Therefore, persistent drought conditions as postulated in this study are possible in the mid- to late-21st century under unmitigated global warming.

Further, it should be noted that the highly impacted southern and southeastern Amazon regions are also the regions that are strongly affected by three additional factors reducing their resilience. First, extended tipping cascades can be expected due to local interaction structures and reduced downwind moisture transport (Figs. 3 and 4). Second, they are also two of the regions located along the "arc of deforestation" and therefore already suffer from the pressure of human-induced activities, such as deforestation, ranching, and extensive agriculture (16, 75, 76). Third, these regions, as well as the whole Amazon rainforest, are threatened by road infrastructure projects (77, 78) and lack of or poorly enforced environmental policies (79, 80).

At the same time, human-induced changes such as deforestation also affect the evapotranspiration negatively, which might then increase the frequency and severity of droughts together with ongoing climate change (43, 81, 82). Besides deforestation, the Amazon rainforest can be impacted adversely by, among others, temperature extremes, fires, or further degradation. But since our aim was to understand the role of tipping events and cascades based on adaptive capacities through the atmospheric moisture recycling network, we tailored our model to the effect of drought-induced instabilities. With this procedure, we are able to find regions where the adaptive capacity might be outpaced under future more consistent droughts. Therefore, these other effects (fire, temperature extremes) are not quantified in this study. Overall, our results emphasize the relevance of the atmospheric moisture recycling network as an ecosystem service whose (partial) breakdown, combined with an increased number of climate-change–induced extreme droughts, could trigger substantial changes across the Amazon basin.

We find that scenarios with higher MCWD anomalies (i.e., that resemble current extreme droughts) show a considerably larger tipped area. Cascading tipping events are more pronounced under these circumstances (Fig. 2). These are the drought conditions that can be expected from midcentury onward if climate change progresses as it would in high-emission scenarios (68–70). The highest response in our model coincides with the strongest El Niño ONI (Oceanic Niño Index) indexes during the period 2004 to 2014 (72). It is known that El Niño-related droughts and other variability patterns affect the stability of the rainforest and tropical vegetation (18, 83). If the anomalies associated with El Niño events intensify as projected by CMIP simulations and perturbed physics models (84, 85), this would endanger substantial portions of the Amazon basin (86). However, uncertainties remain whether strong El Niño events might become more frequent in the future (87). Overall, there is a low level of agreement among CMIP models on projected changes in ENSO (El-Niño Southern Oscillation) variability during the 21st century (88), even though they agree on the drying signal (70).

It is important to note that, while the droughts in 2005 and 2010 show an elevated ENSO-ONI index, they have also been attributed to a warmer tropical and subtropical North Atlantic Ocean (51, 54, 72). Especially the effects on reduced precipitation, leading to reduced atmospheric moisture transport and soil moisture in the arc of deforestation and the central Amazon basin, have been linked to changes in the sea surface temperature in the tropical North Atlantic and the Caribbean (89). Hence a drier future climate over the Amazon is not determined by persistent ENSO conditions.

In our study, we assumed that the forest would undergo a state transition from a forested cell to an only sparsely forested (e.g., open canopy or savanna) or entirely forest-free cell. This is in agreement with a recent model study (90), which shows that a savanna-like state could become stable in most parts of South American tropical forests by the end of the 21st century. However, 1) it has recently been discussed that it may be possible to evade a potential ecological tipping point by the formation of spatial patterns, leading to higher resilience or a more linear change of the system (91), and 2) it could also be possible that the alternative stable state could consist of a dry-forest–like state. Such a species turnover from wet-affiliated to more dry-affiliated tree species is already observed in parts of the Amazon rainforest (37). This would mean that parts of the forest could change to dry forests (4) instead of savanna-like states, but still the forest would undergo a functional and species-compositional shift. Instead of a dry forest, a new social–ecological "equilibrium" state could be driven by land-use change such as agricultural use or pasture. In both cases for dry forests (≈ 750 to $1,000$ mm/y) (92) or pasture and soy (≈ 500 to 700 mm/y) (93), the evapotranspiration could be higher than is assumed in this study after local rainforest collapse. The median value for a scenario resembling 2014, in the case that the rainforest would be collapsed, is around 400 to 500 mm/y of evapotranspiration in our model and is of comparable magnitude to that of pasture or soy (*SI Appendix*, Fig. S10). Still, if the evapotranspiration remains at an even higher level, it is possible that we would overestimate the potential for tipping cascades. To evaluate this, we performed a sensitivity analysis with different strengths of the atmospheric moisture recycling and find a strong robustness of our results (*SI Appendix*, Fig. S5). The corresponding evapotranspiration values for the sensitivity experiment with lower atmospheric moisture recycling values (25% reduction compared to the original values) match the evapotranspiration values of dry forest well (*SI Appendix*, Fig. S10D).

Overall, studies producing transition probability density functions based on the general climatic conditions under which a forest state is possible may be on the conservative side. Such approaches might underestimate the importance of local adaptations or rather the importance of forest diversity. Under the common assumption that trees operate at their maximum performance by optimizing their trade-off affected trait values in a competitive community (40), any significant deviation from common local environmental conditions poses a stress to the established local community (37, 94). It is not that this community can pick from solutions found in the overall pool of trait values in the whole Amazon. The forest community is bound to its local adaptations, i.e., expressions. Even under the assumption of extremely plastic traits, the community would need a lot of time to readjust, which is especially unrealistic for traits like rooting depth or parameters related to wood density (33). Therefore, we view our approach to model adaptation as complementary and a step forward to "potential landscape" methods in earlier studies (9, 17) and expect that the actual tipping points and cascades in the Amazon result from a combination of the crossing of absolute and relative thresholds. Determining these relative effects is a promising avenue for future research as field-based estimates of local tree adaptations are starting to become available. Additionally, parameterizing state transitions across a very broad geographic domain with very diverse climate, species composition, and soil conditions is very challenging, and the details of these parameterizations will strongly impact modeling results. Going forward, more research into this topic seems warranted.

Furthermore, it could be argued that adaptation of trees takes significantly longer than the 20 y we used in our study (control period). In this case, adaptation could have led to a higher resistance in trees against droughts, at least in older trees that have experienced a larger range of different climatic conditions. However, while trees in the Amazon rainforest can easily reach an age of several hundred years, and some up to more than 1,000 y (95), the current rate of climate change is unprecedented in the last 1,000 y and on longer timescales during the Holocene (last 11,700 y) and beyond (88). Therefore, a potential paleo-climate adaptation of trees and with that an adaptation of the overall species composition are very likely exceeded by future climate conditions under global warming. At the same time paleo data on precipitation and evapotranspiration on the required resolution are spotty. Still, for some rainfall stations, it has been found that our dataset is in the same range as precipitation values from the last 100 y (96). While we consider an adaptation of trees to past climatic conditions, it should be noted that the atmospheric moisture network is static and does as such not change during the simulations, e.g., due to a vegetation shift in some rainforest cells. Furthermore, our model should not be seen as a prediction, because it has been developed to be able to perform a risk assessment, finding the most vulnerable regions in response to recurrent droughts.

Another important mechanism has been argued to lie in additional CO_2 fertilization of the vegetation under global warming, accompanied by a potentially more effective intrinsic water-use efficiency of trees (97, 98). However, it is not finally clarified how the balance plays out between the positive effect of CO_2 fertilization and the negative impacts of global warming due to elevated atmospheric carbon levels, which has resulted in increased tree mortality in the Amazon rainforest (99, 100).

Finally, atmospheric moisture export can supply systems that are thousands of kilometers away, implying that forest-induced moisture export is an essential ecological service for regions beyond the Amazon rainforest itself (101). Therefore, the preservation of atmospheric moisture recycling might be considered to play a role in the designation of future protected areas in the Amazon rainforest. Altogether, preserving the Amazon and its ecological services is of utmost importance for local, regional, and global climate stability.

Materials and Methods

Data. The network was constructed using atmospheric moisture-tracking simulations by Staal et al. (42), based on state-of-the-art observation-based moisture-tracking simulations and the hydrological model PCR-GLOBWB (PCRaster GLOBal Water Balance model) forced by Earth Resilience in the Anthropocene ERA-Interim data (102). In that study, first, tree transpiration across South America during 2003 to 2014 was estimated using PCR-GLOBWB. This is a global hydrological model that computes the water balance in two soil layers and a groundwater layer and accounts for soil distributions, fractional area of saturated soil, and spatiotemporal differences in groundwater depth. Next, the atmospheric trajectories of the tree transpiration flux were simulated using a Lagrangian atmospheric moisture-tracking model. This model applies three-dimensional tracking of parcels of moisture that are released in the atmosphere, scaled with the humidity profile of the atmosphere. For the atmospheric fields, data between 1,000 and 500 hPa at 50 hPa vertical resolution were used. At each time step, moisture from the parcels can rain out depending on ERA-Interim precipitation. The model ran with simulation time steps of 0.25 h, where wind speed and direction were interpolated from ERA-Interim reanalysis on 0.75° and 6-h resolution. Moisture parcels were tracked for 30 d or until less than 5% of the original moisture was present. The output is on a monthly basis on 0.25° resolution. Here, we reconstructed those simulation results by taking the atmospheric moisture recycling ratios between 0.25° grid cells, building monthly networks of moisture flows between each pair of cells of a certain resolution for the Amazon region and aggregating them to 1° × 1° grid cells. In addition to tree transpiration, we also included interception evaporation from tree canopies, taken from Staal et al. (2020) (43) on a monthly and 0.5° basis. Furthermore, we accounted for deforestation before and during the study period by subtracting forest-loss results from Hansen et al. (2013) (103), see also Staal et al. (43). We thus obtained temporally varying monthly networks of forest-induced atmospheric moisture flows across the Amazon. For the equations of the Lagrangian moisture-tracking scheme, we refer to Staal et al. (42).

There is still evapotranspiration from the soil left when the forest at a certain grid cell is removed; i.e., tree transpiration and interception evaporation are set to zero. While we do not artificially replace the forest cover by other types of vegetation directly, the leftover evapotranspiration value is on the order of 500 mm/y, which is a bit less (500 to 1,000 mm/y) than the evapotranspiration value of some agricultural crops, pasture, or Cerrado forest (92, 93, 104) (*SI Appendix*, Fig. S10 *A and B*). Therefore, we performed a sensitivity analysis to check whether different values in moisture supply make a difference in the amount of tipping events. By multiplying all links in the atmospheric moisture recycling network by 1) 125% and 2) 75%, we found that the tipped area and the network effects are fully consistent with Fig. 2. Thus, our results are robust for significant differences in moisture transport, also matching the remaining evapotranspiration of dry forests (*SI Appendix*, Figs. S5 and S10*D*).

Monthly precipitation and actual evapotranspiration data for 1984 to 2014 at 0.25° resolution were taken from the ERA5 reanalysis dataset (105), and for robustness comparison in *SI Appendix* from the Famine Early Warning Systems Network Land Data Assimilation System (FLDAS) (106). We have taken 20 y as our adaptation period because in earlier research, 20 y have also been selected as the tree root adaptation time frame, acknowledging that it may be longer (34). Further, the ERA5 and FLDAS data from 1984 to 2003 show a similar range of precipitation values as observational data from across the Amazon basin (96). In this sense, our data also are representative of observational data from earlier times (1920s to 1960s) since 1) there is a similar variability in the precipitation and 2) no strong trend is observed (meaning no decrease or increase in Amazon-wide precipitation over time) (96). In the end, we have chosen the ERA5 data for the main text, but both datasets show robust results, not only with regard to the overall tipping effects, but also with respect to network effects. Also, regional tipping distributions agree fairly well (*SI Appendix*, Fig. S11). Note that all our

simulations are based on hydrological years (starting in October of one calendar year and going to September of the next calendar year) instead of calendar years due to the hydrological cycle over the Amazon basin.

Computation of MAP and MCWD. The MAP is derived from the monthly precipitation values for each cell. The MCWD index is here defined as the absolute value of the most negative value of cumulative water deficit (CWD) reached over a hydrological year:

$$CWD_k = CWD_{k-1} + Precipitation_k - Evapotranspiration_k$$
$$\max(CWD_k) = 0$$
$$MCWD = abs\left(\min\{CWD_k, CWD_{k+1}, \ldots, CWD_{k+12}\}\right), \qquad [1]$$

where k is the number of the month in the hydrological year. We make use of the actual measured regional evapotranspiration values in each grid cell. At the beginning of each hydrological year (i.e., the wettest time of the year) we set CWD_0 to zero, assuming that the soil is saturated, following earlier studies (4). Therefore, this is a conservative measure because legacy effects from drought conditions in preceding years are not accounted for.

There are several other indexes besides MCWD such as the standardized precipitation index (SPI), the standardized precipitation evapotranspiration index (SPEI), and the Linacre water-limitation index (LINACRE) (107, 108). However, we have used the MCWD index in this study since it has been linked to a potential climate-change–induced dieback of parts of the Amazon rainforest in earlier research (4). Furthermore, anomalies from a decadal reference period in MCWD have been shown to correlate positively with drought-induced tree mortality (49, 109), and finally former studies on tropical forest bistability have also made use of the MCWD drought index (9, 43, 90). Note that a comparison between the SPI and MCWD indexes exists (48).

Computation of the $\mathcal{Z}$ Score. The $\mathcal{Z}$ score is used to find the ranges of future conditions that we are simulating in this work. We simulate ranges from current conditions up to extreme droughts that are 3.0 SDs away from the mean (Fig. 2). The MCWD-based $\mathcal{Z}$ score is computed by

$$\mathcal{Z}_{MCWD} = \frac{MCWD(year) - \mu_{MCWD}}{\sigma_{MCWD}}. \qquad [2]$$

Here, μ_{MCWD} and σ_{MCWD} are the average and SD of the calibration period from 1984 to 2003. MCWD(year) is the average MCWD of the specific investigated year (*Materials and Methods*, Computation of MAP and MCWD). For comparison, the $\mathcal{Z}$ score based on MAP is computed (Eq. **3**) and plotted for comparison, and a similar relationship between tipped area and a higher MAP-based score is visible (*SI Appendix*, Fig. S4), but MAP is no reason for tipping (Fig. 3):

$$\mathcal{Z}_{MAP} = \frac{MAP(year) - \mu_{MAP}}{\sigma_{MAP}}. \qquad [3]$$

Adaptation and Computation of Critical Thresholds. Even though there might be absolute thresholds at play in the Amazon rainforest (7, 8, 90), modeling approaches that ignore the possibility of local adaptation may lead to incorrect estimates of tipping points and tipping cascades. Forests are not everywhere equally adapted to local climate conditions (33, 39). There are many strategies within and among forests to cope with, e.g., dry seasons or droughts (34). Our working hypothesis is that local climate conditions must have led to certain forest trait adaptations along the logical lines of environmental filtering, competitive exclusion, and resilience.

For our purpose of computing local adaptation values (local means here based on a $1° \times 1°$ grid), we use a calibration dataset from ERA5 from the hydrological years 1984 to 2003. From there, we compute the 20-y long-term mean of MAP and MCWD values together with their SDs (*SI Appendix*, Fig. S9). The critical value for MAP and MCWD where a state transition occurs is computed for each grid cell i as

$$MAP_{crit,i} = \mu_{MAP,i} - \alpha_i \cdot \sigma_{MAP,i}$$
$$MCWD_{crit,i} = \mu_{MCWD,i} + \alpha_i \cdot \sigma_{MCWD,i}. \qquad [4]$$

μ_i is the mean, σ_i the SD of cell i, and α_i an adaptation factor that determines the exact value of the tipping point. Our procedure leads to the effect that regions with a high MAP as, e.g., in the central Amazon region can only be sustained at higher MAP values compared to other, typically drier regions, for instance, in the south of the Amazon basin or close to the Andes. This means that forests in typically drier regions (e.g., in the southeast of the Amazon basin) can survive with less moisture than forests in wetter regions. The same arguments are valid for MCWD, with regional differences from MAP.

Furthermore, higher variability, i.e., a larger SD, in a region leads to higher adaptation percentage-wise (training effect). In turn, this would also suggest that regions with a very low SD (e.g., where $3\sigma < 30$ mm/y; *SI Appendix*, Fig. S9D) in the central Amazon would shift their state under very small MCWD shocks. It is unlikely from an ecological perspective that those small MCWD shocks would lead to an ecosystem transition, and indeed, in our simulations, we only rarely find tipping events in those low-SD regions due to sufficient precipitation supply. However, once environmental conditions in these regions become significantly drier, then local adaptation might become a curse instead of a blessing, especially in regions with low variability. To stay competitive, very shallow rooting depths should be expected in regions where MCWD is zero (34). A significant deviation from the always wet upper soil layer, for which MCWD is a proxy, for many consecutive years would very likely have significant consequences.

Altogether, we view our adaptation approach as complementary to and a step forward from potential-landscape methods in earlier studies (9, 17) and expect that the actual tipping points and tipping cascades in the Amazon result from a combination of the crossing of absolute and relative thresholds. Determining these relative effects is a promising avenue for future research as field-based estimates of local tree adaptations are starting to become available. Specifically, we see several arguments bringing our approach in line with current literature: 1) Adaptation to climatic and environmental conditions is key to survival of certain tree species and, as such, affects the resilience to climatic changes in the Amazon rainforest (17, 32); 2) those adaptive capacities have in particular been related to tree strategies to cope with droughts (35, 71), but it has been found that tree mortality risks increase when the trees experience climatic conditions outside their adaptive limits (59, 94); and 3) it has been found that even occasional strong droughts have long-lasting impacts on drought-induced tree mortality (57), and vegetation conversions have been observed in multiple biomes worldwide including the Amazon (59, 66).

Dependence on Adaptation Values. With our settings, we can now compute what would happen under sustained conditions that resemble the yearly conditions observed in a particular hydrological year of our study period from 2004 to 2014. In our experiments, we assume that each cell starts with full forest cover (state = 1.0) at $t = 0$. If we are taking the precipitation, evapotranspiration, and atmospheric moisture recycling network of a certain year, then we will find some cells that are unstable since their MAP or, mostly, their MCWD value is below the critical value (Eq. **4**), which is defined with the time series from 1984 to 2003 (*SI Appendix*, Fig. S12 for ERA5 data and FLDAS in *SI Appendix*, Fig. S13). If this is the case, this cell transgresses its threshold and becomes forest cover-free, which then leads to reduced atmospheric moisture recycling since the atmospheric moisture transport value is multiplied by the fraction of forest cover. This means that the atmospheric moisture transport value for tree transpiration and interception evaporation is set to zero when a forested cell tipped. This can then drive further cells toward or across their tipping point such that cascading events can be expected. In the case that a cell is only driven toward, but not across its tipping point, the effects on atmospheric moisture recycling and tree cover are still accounted for, assuming that the response of the vegetation is linearly represented by the state, instead of this effect being zero as in threshold-only models (9).

The critical values depend on the level of locally different adaptation values α_i (Eq. **4**). Thus, it can be expected that a higher adaptation factor leads to a lower number of tipped rainforest cells and vice versa. To check this, we performed a sensitivity experiment, where the adaptation values are the same across the entire Amazon ($\alpha_i = \alpha \ \forall i$). We performed this sensitivity experiment for 0.3, 0.4, . . . 3.0 SDs. We find that the tipped area indeed goes down with increased adaptation factors (*SI Appendix*, Fig. S14A) and observe that the southern and (to a lesser extent) the western regions in the Amazon rainforest are most vulnerable (*SI Appendix*, Fig. S14B). In reality, the true value of adaptation of a certain cell

is unknown and might vary from location to location. That is why a different ensemble of simulations with increased robustness is required and the constant adaptation factor hypothesis ($\alpha = \alpha_i \, \forall i$) is dropped in favor of an ensemble approach where α_i is varied locally. Thus, we create a Monte Carlo ensemble with 100 ensemble members for each year in the study period.

Ensemble Construction. Eq. **4** determines the critical values for MAP and MCWD for each $1° \times 1°$ cell separately. The critical value is dependent on the local average value as well as the variability of the 20 y before the study period (ERA5 data from 1984 to 2003). The exact critical value is determined by the adaptation factor α and must in turn be chosen appropriately. Therefore, we assume that a cell is on average able to remain in the same state under MAP and MCWD conditions that are 2 SDs away from their mean, i.e., from their "experiences" during the previous 20 y. However, as argued above, the exact value of adaptation is uncertain and might be different in different regions, also due to several factors that we do not model explicitly in this work. But we take this into account by drawing the individual adaptation values α_i for each cell i from a β-distribution that is centered at 2 SDs and ranges from 1 to 3 SDs:

$$\beta(x, a, b) = (\sigma_{\text{upper}} - \sigma_{\text{lower}}) \cdot \frac{x^{a-1}(1-x)^{b-1}}{\int_0^1 t^{a-1}(t-1)^{b-1}dt} + \sigma_{\text{lower}}. \quad \textbf{[5]}$$

Here, we use $\sigma_{\text{upper}} = 3.0$ and $\sigma_{\text{lower}} = 1.0$ for the upper and lower bounds. We choose $a = b = 2.5$, which ensures that, on average, 75% of all values lie between 1.5 and 2.5 SDs and 12.5% lie between 1.0 and 1.5 or between 2.5 and 3.0 SDs, respectively. This means that 75% lie in the central interval and 25% outside (75 to 25 rule). We have taken 2 SDs as our central estimate in this study and have chosen a β-distribution since it is analogous to a normal distribution for a fixed interval. With that procedure we construct an ensemble of 100 members of which 3 examples can be found in *SI Appendix*, Fig. S15. If not stated otherwise, all results shown are from the average over the 100 ensemble members.

Network of Coupled Nonlinear Differential Equations. We use a combination of nonlinear differential equations together with a complex network to describe the state of the rainforest cells and their interactions (110). We use this approach instead of a threshold approach since we want to be able to account for partial changes in the state and their effects on the network. For instance, such changes can be critical for the tipping of cells that are not coupled directly, but via an intermediary cell, where partial changes are decisive for the emergence of a tipping cascade. Indirect effects have been found to account for 10% and more, already in very simple interaction structures in so-called motifs (111).

In the differential equation approach in this work, we model the main hydrological parameters and the stability of the rainforest, but no further parameters such as biotic variables or further ecophysiological processes. The main hydrological properties are the precipitation (MAP), the MCWD, and the atmospheric moisture recycling. Following the reasoning above, we describe the mathematical details in the remainder of this section.

Each $1° \times 1°$ cell is represented by a differential equation of the form

$$\frac{dx_i}{dt} = x_i^3 - x_i + \mathcal{F}_{\text{crit}}(\text{MAP}_i, \text{MCWD}_i), \quad \textbf{[6]}$$

where x_i stands for the state of the rainforest cell and can be interpreted as the fraction of tree cover. The shape of this function can be seen in *SI Appendix*, Fig. S16. Furthermore, Eq. **6** has the normal form of a saddle-node bifurcation and is a simple form of a differential equation with two stable states. Such equations have been used to model dynamics in various contexts such as economics, ecology, and the Earth system (112, 113). The two states are stable depending on the value of the critical function $\mathcal{F}_{\text{crit}}$, where $+1.0$ stands for full tree cover and -1.0 for the alternative state without full tree cover. Such an alternative state could be a savanna-like state or completely treeless. It is not possible for a cell to have lower tree cover values than 0% or values higher than full forest cover such that the state x_i is limited to the interval $[-1.0, 1.0]$. The advantage of choosing state limits of -1.0 and $+1.0$

is that the critical value then remains analytically representable and has the specific value $\mathcal{C}_{\text{crit}} = \sqrt{4/27}$ (*SI Appendix*, Fig. S16). This value is derived from the discriminant of the polynomial of Eq. **6**. More details can be found in the literature (112, 114). For other state limits such as between 0.0 and 1.0, this would have to be dropped since the parameters in front of the cubic and linear terms of Eq. **6** would be different. Therefore, we decided for prefactors of 1.0 in front of the cubic and the linear term such that the state limits are -1.0 and $+1.0$. As soon as the critical value of $\mathcal{C}_{\text{crit}}$ is reached by $\mathcal{F}_{\text{crit}}$, a state transition will occur since the upper stable state becomes unstable and only the lower stable state remains stable. For more details on this equation and the critical value, see Wunderling et al. (111) and Klose et al. (112).

In our case, the rainforest cells are not independent, but interact via atmospheric moisture recycling such that Eq. **6** becomes

$$\frac{dx_i}{dt} = x_i^3 - x_i + \mathcal{F}_{\text{crit}}(\text{MAP}_i, \text{MCWD}_i)$$
$$+ \sum_{\substack{j=1 \\ j \neq i}}^{N} \mathcal{M}_{ji}(\Delta\text{MAP}_{ji}, \Delta\text{MCWD}_{ji}) \frac{x_j}{2}. \quad \textbf{[7]}$$

Here, the entries of the critical matrix $\mathcal{M}_{ji}(\Delta\text{MAP}_{ji}, \Delta\text{MCWD}_{ji})$ represent the strength of the atmospheric moisture recycling link between two grid cells from j to i. The state x_j must be divided by 2 since the distance from the minimum to the maximum state is 2. Similar forms of the network and the differential equation have already been used in earlier studies in the literature, but in a more simplified form than in this work (47, 111). For the computation of the critical function $\mathcal{F}_{\text{crit}}(\text{MAP}_i, \text{MCWD}_i)$ and the critical (interaction) matrix $\mathcal{M}_{ji}(\Delta\text{MAP}_{ji}, \Delta\text{MCWD}_{ji})$, see *SI Appendix, Methods*.

Resolution Independence. To check for robustness of our results, we recomputed our simulations with respect to the resolutions of $1.5° \times 1.5°$ and $2° \times 2°$ (*SI Appendix*, Figs. S17 and S18). For that purpose, we scale the minimal atmospheric moisture recycling value connecting to rainforest cells with the area of a cell. In the case of a resolution of $1° \times 1°$ we take all values above 1.0 mm/y into account, for $1.5° \times 1.5°$ all values above 2.25 mm/y, and for $2° \times 2°$ all values above 4.0 mm/y. Overall, we find that the vulnerability patterns are spatially similar (compare Fig. 3*A* with *SI Appendix*, Fig. S17). Thus, the qualitative pattern is the same. The absolute values also show a close quantitative match within their SDs for all resolutions (*SI Appendix*, Fig. S18).

Notes on Color Maps. This paper makes use of perceptually uniform color maps developed by F. Crameri (115).

Author affiliations: [a]Earth System Analysis, Potsdam Institute for Climate Impact Research, Member of the Leibniz Association, 14473 Potsdam, Germany; [b]Institute of Physics and Astronomy, University of Potsdam, 14476 Potsdam, Germany; [c]Department of Physics, Humboldt University of Berlin, 12489 Berlin, Germany; [d]Copernicus Institute of Sustainable Development, Utrecht University, Utrecht, 3584 CB, The Netherlands; [e]Stockholm Resilience Centre, Stockholm University, Stockholm, SE-10691, Sweden; [f]Department of Physics, Federal University of Santa Catarina, Florianópolis 88040-900-SC, Brasil; [g]Department of Plant Biology, University of Campinas, Campinas 13083-970-SP, Brasil; [h]Instituto de Física, Universidade de São Paulo, São Paulo 05508-090-SP, Brasil; and [i]Physics Department, University of Maryland Baltimore County, Baltimore, MD 21250

1. J. Barlow et al., The future of hyperdiverse tropical ecosystems. Nature **559**, 517–526 (2018).
2. E. T. A. Mitchard, The tropical forest carbon cycle and climate change. Nature **559**, 527–534 (2018).
3. C. A. Nobre et al., Land-use and climate change risks in the Amazon and the need of a novel sustainable development paradigm. Proc. Natl. Acad. Sci. U.S.A. **113**, 10759–10768 (2016).
4. Y. Malhi et al., Exploring the likelihood and mechanism of a climate-change-induced dieback of the Amazon rainforest. Proc. Natl. Acad. Sci. U.S.A. **106**, 20610–20615 (2009).
5. L. F. Salazar, C. A. Nobre, Climate change and thresholds of biome shifts in Amazonia. Geophys. Res. Lett. **37**, 17706 (2010).
6. M. D. Oyama, C. A. Nobre, A new climate-vegetation equilibrium state for tropical South America. Geophys. Res. Lett. **30**, 2199 (2003).
7. A. C. Staver, S. Archibald, S. A. Levin, The global extent and determinants of savanna and forest as alternative biome states. Science **334**, 230–232 (2011).
8. M. Hirota, M. Holmgren, E. H. van Nes, M. Scheffer, Global resilience of tropical forest and savanna to critical transitions. Science **334**, 232–235 (2011).
9. D. C. Zemp et al., Self-amplified Amazon forest loss due to vegetation-atmosphere feedbacks. Nat. Commun. **8**, 14681 (2017).
10. A. Staal, S. C. Dekker, M. Hirota, E. H. van Nes, Synergistic effects of drought and deforestation on the resilience of the south-eastern Amazon rainforest. Ecol. Complex. **22**, 65–75 (2015).
11. E. H. van Nes, M. Hirota, M. Holmgren, M. Scheffer, Tipping points in tropical tree cover: Linking theory to data. Glob. Change Biol. **20**, 1016–1021 (2014).
12. P. Meir et al., Threshold responses to soil moisture deficit by trees and soil in tropical rain forests: Insights from field experiments. Bioscience **65**, 882–892 (2015).
13. L. Rowland et al., Death from drought in tropical forests is triggered by hydraulics not carbon starvation. Nature **528**, 119–122 (2015).
14. T. M. Lenton et al., Tipping elements in the Earth's climate system. Proc. Natl. Acad. Sci. U.S.A. **105**, 1786–1793 (2008).
15. T. E. Lovejoy, C. Nobre, Amazon tipping point: Last chance for action. Sci. Adv. **5**, eaba2949 (2019).
16. C. A. Boulton, T. M. Lenton, N. Boers, Pronounced loss of Amazon rainforest resilience since the early 2000s. Nat. Clim. Chang. **12**, 271–278 (2022).
17. C. Ciemer et al., Higher resilience to climatic disturbances in tropical vegetation exposed to more variable rainfall. Nat. Geosci. **12**, 174–179 (2019).
18. M. Holmgren, M. Hirota, E. H. van Nes, M. Scheffer, Effects of interannual climate variability on tropical tree cover. Nat. Clim. Chang. **3**, 755–758 (2013).
19. R. Fu et al., Increased dry-season length over southern Amazonia in recent decades and its implication for future climate projection. Proc. Natl. Acad. Sci. U.S.A. **110**, 18110–18115 (2013).
20. J. A. Marengo et al., Changes in climate and land use over the Amazon region: Current and future variability and trends. Front. Earth Sci. **6**, 228 (2018).
21. I. C. Correa, P. A. Arias, M. Rojas, Evaluation of multiple indices of the South American monsoon. Int. J. Climatol. **41**, E2801–E2819 (2020).
22. J. C. Espinoza, J. Ronchail, J. A. Marengo, H. Segura, Contrasting North–South changes in Amazon wet-day and dry-day frequency and related atmospheric features (1981–2017). Clim. Dyn. **52**, 5413–5430 (2019).
23. D. Arvor, B. M. Funatsu, V. Michot, V. Dubreuil, Monitoring rainfall patterns in the southern Amazon with PERSIANN-CDR data: Long-term characteristics and trends. Remote Sens. **9**, 889 (2017).
24. A. Lopes, J. Chiang, S. Thompson, J. Dracup, Trend and uncertainty in spatial-temporal patterns of hydrological droughts in the Amazon basin. Geophys. Res. Lett. **43**, 3307–3316 (2016).
25. P. A. Arias, R. Fu, C. Vera, M. Rojas, A correlated shortening of the North and South American monsoon seasons in the past few decades. Clim. Dyn. **45**, 3183–3203 (2015).
26. L. Giráldez, Y. Silva, R. Zubieta, J. Sulca, Change of the rainfall seasonality over central Peruvian Andes: Onset, end, duration and its relationship with large-scale atmospheric circulation. Climate (Basel) **8**, 23 (2020).
27. N. Haghtalab, N. Moore, B. P. Heerspink, D. W. Hyndman, Evaluating spatial patterns in precipitation trends across the Amazon basin driven by land cover and global scale forcings. Theor. Appl. Climatol. **140**, 1–17 (2020).
28. N. S. Debortoli et al., Rainfall patterns in the Southern Amazon: A chronological perspective (1971–2010). Clim. Change **132**, 251–264 (2015).
29. J. P. Boisier, P. Ciais, A. Ducharne, M. Guimberteau, Projected strengthening of Amazonian dry season by constrained climate model simulations. Nat. Clim. Chang. **5**, 656–660 (2015).
30. E. Joetzjer, H. Douville, C. Delire, P. Ciais, Present-day and future Amazonian precipitation in global climate models: CMIP5 versus CMIP3. Clim. Dyn. **41**, 2921–2936 (2013).
31. R. S. Oliveira et al., Linking plant hydraulics and the fast-slow continuum to understand resilience to drought in tropical ecosystems. New Phytol. **230**, 904–923 (2021).
32. B. Sakschewski et al., Resilience of Amazon forests emerges from plant trait diversity. Nat. Clim. Chang. **6**, 1032–1036 (2016).
33. B. Sakschewski et al., Variable tree rooting strategies are key for modelling the distribution, productivity and evapotranspiration of tropical evergreen forests. Biogeosciences **18**, 4091–4116 (2021).
34. C. Singh, L. Wang-Erlandsson, I. Fetzer, J. Rockström, R. van der Ent, Rootzone storage capacity reveals drought coping strategies along rainforest-savanna transitions. Environ. Res. Lett. **15**, 124021 (2020).
35. F. V. Barros et al., Hydraulic traits explain differential responses of Amazonian forests to the 2015 El Niño-induced drought. New Phytol. **223**, 1253–1266 (2019).
36. A. Esquivel-Muelbert et al., Seasonal drought limits tree species across the Neotropics. Ecography **40**, 618–629 (2017).
37. A. Esquivel-Muelbert et al., Compositional response of Amazon forests to climate change. Glob. Change Biol. **25**, 39–56 (2019).
38. W. R. L. Anderegg et al., Hydraulic diversity of forests regulates ecosystem resilience during drought. Nature **561**, 538–541 (2018).
39. C. Singh, R. van der Ent, L. Wang-Erlandsson, I. Fetzer, Hydroclimatic adaptation critical to the resilience of tropical forests. Glob. Chang. Biol. **28**, (2022).
40. B. Choat et al., Global convergence in the vulnerability of forests to drought. Nature **491**, 752–755 (2012).
41. L. E. Aragão, Environmental science: The rainforest's water pump. Nature **489**, 217–218 (2012).
42. A. Staal et al., Forest-rainfall cascades buffer against drought across the Amazon. Nat. Clim. Chang. **8**, 539–543 (2018).
43. A. Staal et al., Feedback between drought and deforestation in the Amazon. Environ. Res. Lett. **15**, 044024 (2020).
44. J. Agudelo, P. A. Arias, S. C. Vieira, J. A. Martínez, Influence of longer dry seasons in the Southern Amazon on patterns of water vapor transport over northern South America and the Caribbean. Clim. Dyn. **52**, 2647–2665 (2019).
45. M. Ruiz-Vásquez, P. A. Arias, J. A. Martínez, J. C. Espinoza, Effects of Amazon basin deforestation on regional atmospheric circulation and water vapor transport towards tropical South America. Clim. Dyn. **54**, 4169–4189 (2020).
46. A. L. Swann, M. Longo, R. G. Knox, E. Lee, P. R. Moorcroft, Future deforestation in the Amazon and consequences for South American climate. Agric. For. Meteorol. **214**, 12–24 (2015).
47. J. Krönke et al., Dynamics of tipping cascades on complex networks. Phys. Rev. E **101**, 042311 (2020).
48. L. O. Anderson et al., Vulnerability of Amazonian forests to repeated droughts. Philos. Trans. R. Soc. Lond. B Biol. Sci. **373**, 20170411 (2018).
49. S. L. Lewis, P. M. Brando, O. L. Phillips, G. M. van der Heijden, D. Nepstad, The 2010 Amazon drought. Science **331**, 554 (2011).
50. J. S. Panisset et al., Contrasting patterns of the extreme drought episodes of 2005, 2010 and 2015 in the Amazon basin. Int. J. Climatol. **38**, 1096–1104 (2018).
51. J. A. Marengo, J. Tomasella, L. M. Alves, W. R. Soares, D. A. Rodriguez, The drought of 2010 in the context of historical droughts in the Amazon region. Geophys. Res. Lett. **38**, L12703 (2011).
52. J. C. Espinoza et al., Climate variability and extreme drought in the upper Solimões River (western Amazon basin): Understanding the exceptional 2010 drought. Geophys. Res. Lett. **38**, L13406 (2011).
53. T. Feldpausch et al., Amazon forest response to repeated droughts. Global Biogeochem. Cycles **30**, 964–982 (2016).
54. J. A. Marengo, C. A. Nobre, J. Tomasella, M. F. Cardoso, M. D. Oyama, Hydro-climate and ecological behaviour of the drought of Amazonia in 2005. Philos. Trans. R. Soc. Lond. B Biol. Sci. **363**, 1773–1778 (2008).
55. C. E. Doughty et al., Drought impact on forest carbon dynamics and fluxes in Amazonia. Nature **519**, 78–82 (2015).
56. L. V. Gatti et al., Drought sensitivity of Amazonian carbon balance revealed by atmospheric measurements. Nature **506**, 76–80 (2014).
57. P. M. Brando et al., Abrupt increases in Amazonian tree mortality due to drought-fire interactions. Proc. Natl. Acad. Sci. U.S.A. **111**, 6347–6352 (2014).
58. L. M. Müller, M. Bahn, Drought legacies and ecosystem responses to subsequent drought. Glob. Chang. Biol. (2022).
59. A. Esquivel-Muelbert et al., Tree mode of death and mortality risk factors across Amazon forests. Nat. Commun. **11**, 5515 (2020).
60. P. M. Brando et al., Drought effects on litterfall, wood production and belowground carbon cycling in an Amazon forest: Results of a throughfall reduction experiment. Philos. Trans. R. Soc. Lond. B Biol. Sci. **363**, 1839–1848 (2008).
61. R. Fisher et al., The response of an Eastern Amazonian rain forest to drought stress: Results and modelling analyses from a throughfall exclusion experiment. Glob. Change Biol. **13**, 2361–2378 (2007).
62. D. C. Nepstad, I. M. Tohver, D. Ray, P. Moutinho, G. Cardinot, Mortality of large trees and lianas following experimental drought in an Amazon forest. Ecology **88**, 2259–2269 (2007).
63. X. Wang et al., Hydroclimate changes across the Amazon lowlands over the past 45,000 years. Nature **541**, 204–207 (2017).

64. C. Nobre et al., Science Panel for the Amazon: Amazon Assessment Report 2021 (United Nations Sustainable Development Solutions Network, New York, NY, 2021), chap. 24.

65. B. M. Flores, M. Holmgren, White-sand savannas expand at the core of the Amazon after forest wildfires. Ecosystems 24, 1624–1637 (2021).

66. E. Batllori et al., Forest and woodland replacement patterns following drought-related mortality. Proc. Natl. Acad. Sci. U.S.A. 117, 29720–29729 (2020).

67. P. B. Duffy, P. Brando, G. P. Asner, C. B. Field, Projections of future meteorological drought and wet periods in the Amazon. Proc. Natl. Acad. Sci. U.S.A. 112, 13172–13177 (2015).

68. P. M. Cox et al., Increasing risk of Amazonian drought due to decreasing aerosol pollution. Nature 453, 212–215 (2008).

69. B. Cook et al., Twenty-first century drought projections in the CMIP6 forcing scenarios. Earth's Futur. 8, e2019EF001461 (2020).

70. L. Parsons, Implications of CMIP6 projected drying trends for 21st century Amazonian drought risk. Earth's Futur. 8, e2020EF001608 (2020).

71. M. Brum et al., Hydrological niche segregation defines forest structure and drought tolerance strategies in a seasonal Amazon forest. J. Ecol. 107, 318–333 (2019).

72. J. A. Marengo, J. C. Espinoza, Extreme seasonal droughts and floods in Amazonia: Causes, trends and impacts. Int. J. Climatol. 36, 1033–1050 (2016).

73. E. E. Maeda, H. Kim, L. E. Aragão, J. S. Famiglietti, T. Oki, Disruption of hydroecological equilibrium in southwest Amazon mediated by drought. Geophys. Res. Lett. 42, 7546–7553 (2015).

74. N. Restrepo-Coupe et al., What drives the seasonality of photosynthesis across the Amazon basin? A cross-site analysis of eddy flux tower measurements from the Brasil flux network. Agric. For. Meteorol. 182, 128–144 (2013).

75. E.J.d.A.L. Pereira, L. C. de Santana Ribeiro, L. F. da Silva Freitas, H. B. de Barros Pereira, Brazilian policy and agribusiness damage the Amazon rainforest. Land Use Policy 92, 104491 (2020).

76. E. A. Davidson et al., The Amazon basin in transition. Nature 481, 321–328 (2012).

77. L. Ferrante, P. M. Fearnside, The Amazon's road to deforestation. Science 369, 634 (2020).

78. M. dos Santos Júnior et al., BR-319 como Propulsora de Desmatamento: Simulando o Impacto da Rodovia Manaus-Porto Velho (Instituto do Desenvolvimento Sustentável da Amazon, 2018) ().

79. L. M. Diele-Viegas, E.J.d.A.L. Pereira, C.F.D. Rocha, The new Brazilian gold rush: Is Amazonia at risk? For. Policy Econ. 119, 102270 (2020).

80. P. Artaxo, Working together for Amazonia. Science 363, 323 (2019).

81. J. Q. Chambers, P. Artaxo, Biosphere–atmosphere interactions: Deforestation size influences rainfall. Nat. Clim. Chang. 7, 175–176 (2017).

82. C. D'Almeida et al., The effects of deforestation on the hydrological cycle in Amazonia: A review on scale and resolution. Int. J. Climatol. A J. R. Meteorol. Soc. 27, 633–647 (2007).

83. Y. Malhi, J. Wright, Spatial patterns and recent trends in the climate of tropical rainforest regions. Philos. Trans. R. Soc. Lond. B Biol. Sci. 359, 311–329 (2004).

84. W. Cai et al., ENSO and greenhouse warming. Nat. Clim. Chang. 5, 849–859 (2015).

85. W. Cai et al., Increasing frequency of extreme El Niño events due to greenhouse warming. Nat. Clim. Chang. 4, 111–116 (2014).

86. M. Duque-Villegas, J. F. Salazar, A. M. Rendón, Tipping the ENSO into a permanent El-Niño can trigger state transitions in global terrestrial ecosystems. Earth Syst. Dyn. 10, 631–650 (2019).

87. M. Collins et al., The impact of global warming on the tropical Pacific Ocean and El Niño. Nat. Geosci. 3, 391–397 (2010).

88. V. Masson-Delmotte et al., "Climate change 2021: The physical science basis" in Contribution of Working Group I to the Sixth Assessment Report of the Intergovernmental Panel on Climate Change (Cambridge University Press, Cambridge, UK, 2021), pp. 1–31, 553–672.

89. P. A. Arias et al., Changes in normalized difference vegetation index in the Orinoco and Amazon River basins: Links to tropical Atlantic surface temperatures. J. Clim. 33, 8537–8559 (2020).

90. A. Staal et al., Hysteresis of tropical forests in the 21st century. Nat. Commun. 11, 4978 (2020).

91. M. Rietkerk et al., Evasion of tipping in complex systems through spatial pattern formation. Science 374, eabj0359 (2021).

92. M. Jung et al., Recent decline in the global land evapotranspiration trend due to limited moisture supply. Nature 467, 951–954 (2010).

93. G. de Oliveira et al., Evapotranspiration and precipitation over pasture and soybean areas in the Xingu River basin, an expanding Amazonian agricultural frontier. Agronomy 10, 1112 (2020).

94. K. G. Dexter et al., Inserting tropical dry forests into the discussion on biome transitions in the tropics. Front. Ecol. Evol. 6, 104 (2018).

95. S. Vieira et al., Slow growth rates of Amazonian trees: Consequences for carbon cycling. Proc. Natl. Acad. Sci. U.S.A. 102, 18502–18507 (2005).

96. P. Satyamurty, A. A. de Castro, J. Tota, L. E. da Silva Gularte, A. O. Manzi, Rainfall trends in the Brazilian Amazon basin in the past eight decades. Theor. Appl. Climatol. 99, 139–148 (2010).

97. J. M. Mathias, R. B. Thomas, Global tree intrinsic water use efficiency is enhanced by increased atmospheric CO_2 and modulated by climate and plant functional types. Proc. Natl. Acad. Sci. U.S.A. 118, e2014286118 (2021).

98. W. Hubau et al., Asynchronous carbon sink saturation in African and Amazonian tropical forests. Nature 579, 80–87 (2020).

99. R. J. Brienen et al., Long-term decline of the Amazon carbon sink. Nature 519, 344–348 (2015).

100. D. Schimel, B. B. Stephens, J. B. Fisher, Effect of increasing CO2 on the terrestrial carbon cycle. Proc. Natl. Acad. Sci. U.S.A. 112, 436–441 (2015).

101. R. van der Ent, H. Savenije, Length and time scales of atmospheric moisture recycling. Atmos. Chem. Phys. 11, 1853–1863 (2011).

102. E. H. Sutanudjaja et al., PCR-GLOBWB2: A 5 arcmin global hydrological and water resources model. Geosci. Model Dev. 11, 2429–2453 (2018).

103. M. C. Hansen et al., High-resolution global maps of 21st-century forest cover change. Science 342, 850–853 (2013).

104. B. O. Christoffersen et al., Mechanisms of water supply and vegetation demand govern the seasonality and magnitude of evapotranspiration in Amazonia and Cerrado. Agric. For. Meteorol. 191, 33–50 (2014).

105. European Centre for Medium-Range Weather Forecasts, Fifth generation of ECMWF atmospheric reanalyses of the global climate (ERA5), Copernicus Climate Change Service Climate Data Store (CDS) (2017). https://cds.climate.copernicus.eu/cdsapp#home. Accessed 17 February 2022.

106. A. McNally, NASA/GSFC/HSL, FLDAS Noah Land Surface Model L4 Global Monthly 0.1x0.1 degree (MERRA-2 and CHIRPS), Goddard Earth Sciences Data and Information Services Center (GES DISC) (2018). 10.5067/5nhc22t9375g. Accessed 17 February 2022.

107. J. M. Nogueira, S. Rambal, J. P. R. Barbosa, F. Mouillot, Spatial pattern of the seasonal drought/burned area relationship across Brazilian biomes: Sensitivity to drought metrics and global remote-sensing fire products. Climate (Basel) 5, 42 (2017).

108. S. M. Vicente-Serrano et al., Performance of drought indices for ecological, agricultural, and hydrological applications. Earth Interact. 16, 1–27 (2012).

109. O. L. Phillips et al., Drought sensitivity of the Amazon rainforest. Science 323, 1344–1347 (2009).

110. N. Wunderling et al., Modelling nonlinear dynamics of interacting tipping elements on complex networks: The pycascades package. Eur. Phys. J. Spec. Top. 230, 3163–3176 (2021).

111. N. Wunderling et al., How motifs condition critical thresholds for tipping cascades in complex networks: Linking micro-to macro-scales. Chaos 30, 043129 (2020).

112. A. K. Klose, V. Karle, R. Winkelmann, J. F. Donges, Emergence of cascading dynamics in interacting tipping elements of ecology and climate. R. Soc. Open Sci. 7, 200599 (2020).

113. C. D. Brummitt, G. Barnett, R. M. D'Souza, Coupled catastrophes: Sudden shifts cascade and hop among interdependent systems. J. R. Soc. Interface 12, 20150712 (2015).

114. Y. A. Kuznetsov, Elements of Applied Bifurcation Theory, Applied Mathematical Sciences (Springer Science & Business Media, New York, NY, 2004), vol. 112.

115. F. Crameri, Geodynamic diagnostics, scientific visualisation and staglab 3.0. Geosci. Model Dev. 11, 2541–2562 (2018).

116. J. Kroenke, D. Kistinger, J. Donges, N. Wunderling, pycascades - a software package to simulate dynamics of tipping cascades on complex networks. Zenodo. https://zenodo.org/record/4153102. Deposited 29 October 2020.

117. N. Wunderling et al., Amazon Adaptation Model. figshare. https://figshare.com/articles/software/Amazon_Adaptation_Model/20089331. Deposited 17 June 2022.

118. N. Wunderling, "Nichtlineare Dynamiken und Interaktionen von Kippelementen im Erdsystem," PhD thesis, Universität Potsdam, Potsdam, Germany (2021).